Thickness dependence of electron-electron interactions in topological *p-n* junctions

Dirk Backes,[1,2,*] Danhong Huang,[3] Rhodri Mansell,[1] Martin Lanius,[4] Jörn Kampmeier,[4] David Ritchie,[1] Gregor Mussler,[4] Godfrey Gumbs,[5] Detlev Grützmacher,[4] and Vijay Narayan[1,†]

[1]*Cavendish Laboratory, University of Cambridge, J. J. Thomson Avenue, Cambridge CB3 0HE, United Kingdom*
[2]*Department of Physics, Loughborough University, Epinal Way, Loughborough LE11 3TU, United Kingdom*
[3]*Air Force Research Laboratory, Space Vehicles Directorate, Kirtland Air Force Base, New Mexico 87117, USA*
[4]*Peter Grünberg Institute (PGI-9), Forschungszentrum Jülich, 52425 Jülich, Germany*
[5]*Department of Physics and Astronomy, Hunter College of the City University of New York, 695 Park Avenue, New York, New York 10065, USA*

Electron-electron interactions in topological *p-n* junctions consisting of vertically stacked topological insulators are investigated. *n*-type Bi_2Te_3 and *p*-type Sb_2Te_3 of varying relative thicknesses are deposited using molecular beam epitaxy and their electronic properties measured using low-temperature transport. The screening factor is observed to decrease with increasing sample thickness, a finding which is corroborated by semiclassical Boltzmann theory. The number of two-dimensional states determined from electron-electron interactions is larger compared to the number obtained from weak antilocalization, in line with earlier experiments using single layers.

I. INTRODUCTION

Topological insulators are fascinating materials with conducting surfaces, harboring electronic states with a Dirac-like band structure [1]. Large spin-orbit interaction together with time reversal symmetry cause the topological nature of these surface states (TSS), manifesting itself in the suppression of backscattering and leading to the weak-antilocalization effect (WAL) and to spin-momentum coupling. Furthermore, magnetic topological insulators exhibit the quantum anomalous Hall effect [2–4], characterized by dissipationless chiral currents. These properties of topological insulators have attracted great attention because of their potential applications in energy-efficient electronics and quantum computing.

The analysis of the topological properties is complicated by the nonzero conductivity of the bulk [5–7], which often dominates the overall transport characteristics. Several methods have been devised to suppress the bulk contribution, such as doping [8–11], gating [6,12–14], and reducing the thickness of the layer [15]. A relatively unexplored but elegant method is to combine an electron and hole dominated material to form a *p-n* junction, thus creating a depletion layer at the interface [16–18].

The π-Berry phase of the Dirac fermions gives rise to quantum corrections of the conductivity, with a magnetic field and temperature dependence resembling the WAL effect. Additional modifications of the conductivity are caused by electron-electron interactions (EEI), originating from an effective decrease of the electron density at the Fermi level [19–22]. Both WAL and EEI are best studied by observing the magnetoresistance (MR) at low temperatures, revealing information about the spin (EEI) and orbital (WAL) part of

the electron wave function [23]. The MR is typically parabolic for bulk transport but linear in the case of TSS with two-dimensional character. The WAL effect manifests as a dip of the MR around zero field, which can be modelled using the prefactor α, related to the number of 2D states, and the phase coherence length l_ϕ for fitting [24]. This and a linear MR at high magnetic fields are strong evidence for the topological nature of a TI [25,26].

EEI are a potential origin for conductivity corrections below a certain transition temperature. In contrast to the WAL effect, EEI are robust against magnetic fields, and by studying the temperature dependence in a magnetic field the degree of screening present in the sample can be examined. Although the screening factor F can only attain values between 0 (no screening) and 1 (strong screening), negative values have been reported [27]. This rather unphysical outcome can be avoided by allowing more than one channel to participate. Despite the large body of literature only few simultaneous studies of both effects exist [28–39]. Most strikingly, the number of 2D channels contributing to WAL and EEI, n_{WAL} and n_{EEI}, respectively, are different [29–36], with n_{EEI} being larger than n_{WAL} (see Fig. 1 and Table I). It seems that surface states on the top and bottom contribute independently to EEI but that, under certain circumstances, they appear to be coupled when the WAL effect is concerned. The physical origin of this coupling effect remains elusive. Predominantly in very thin layers only one 2D state contributes to WAL [31,34,36,38,39]. Thicker films tend to be decoupled when WAL is concerned and therefore exhibit a higher number of 2D channels [32,35–37]. Microflakes [30] and hot wall epitaxy deposited layers [29] are exceptions where coupling effects can be observed even at thicknesses >60 nm. A combined study of the WAL and EEI in TI multilayers is entirely missing.

In the following, we present an investigation of the interplay of WAL and EEI in topological *p-n* junctions. Conductivity corrections are measured at temperatures <10 K as a
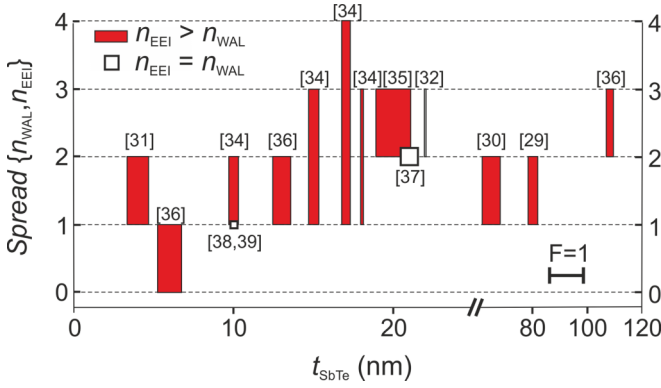
---

*db639@cam.ac.uk
†vn237@cam.ac.uk

FIG. 1. Comparison of the number of 2D channels from WAL (n_{WAL}) and EEI (n_{EEI}) as a function of the layer thickness. The values are taken from literature, with the references given in brackets. The bars indicate the spread between n_{EEI} (top) and n_{WAL} (bottom). Squares indicate experiments where $n_{EEI} = n_{WAL}$. The widths of the bars are proportional to the screening factor F (see scale bar at the bottom right).

function of temperature, magnetic field, and sample thickness. The conductivity corrections are used to find the number of 2D channels contributing to either EEI or WAL. Finally, a semiclassical Boltzmann theory is derived to understand the thickness dependence of the conductivity corrections due to EEI.

II. EXPERIMENT

Bi_2Te_3/Sb_2Te_3 bilayers (BST) were grown using molecular beam epitaxy (MBE). Details of the MBE sample preparation can be found in Ref. [17]. The bottom Bi_2Te_3 layer was 6 nm and the top Sb_2Te_3 layers were 6.6 nm (BST6), 7.5 nm (BST7), 15 nm (BST15), and 25 nm (BST25) thick, respectively. The films were patterned into Hall bars which were 200 μm wide and 1000 μm long [18]. Transport in these samples was measured in a He-3 cryostat at temperature down to 300 mK while a perpendicular magnetic field could be applied using a superconductive magnet.

TABLE I. Sample details of experiments reporting both on WAL and EEI. Most results are obtained using thin films grown by molecular beam epitaxy (MBE) and sputtering (SP) while only a few are based on hot wall epitaxy (HTW) and microflakes.

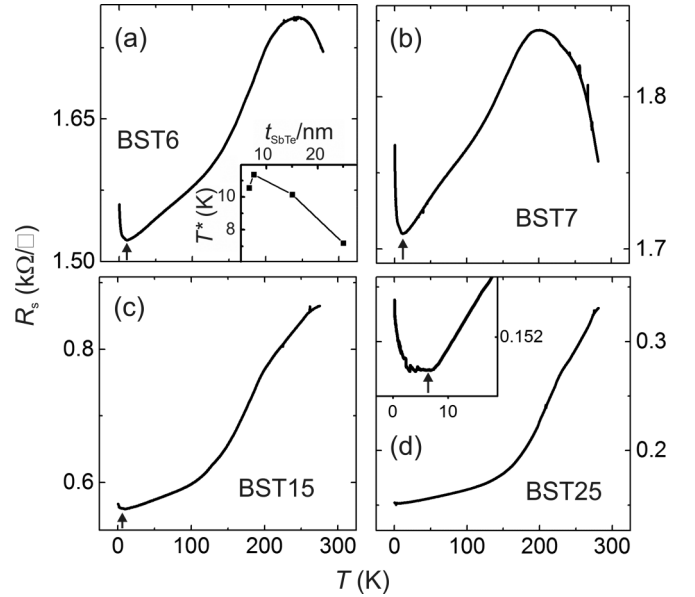| Ref.	Sample	Method	t/nm
Roy *et al.* [31]	BiTe	MBE	4
Wang *et al.* [36]	BiSe	SP	6-108
Jing *et al.* [38]	BiSe	MBE	10
Trivedi *et al.* [39]	BiTeS	Flakes	10
Kuntsevich *et al.* [34]	BiSe	MBE	10-18
Sahu *et al.* [35]	BiSe	SP	20
Takagaki *et al.* [37]	SbTe	MBE	21
Takagaki *et al.* [32]	SbTe	MBE	22
Chiu *et al.* [30]	BiTe	Flakes	65
Takagaki *et al.* [29]	Cu-doped BiSe	HWE	80

FIG. 2. (a)–(d) Sheet resistance R_s dependance on temperature for four different samples. The arrows indicate the transition temperature T^*. Inset in (a): Transition temperature T^* dependence on thickness of the Sb_2Te_3 layer.

In previous experiments, the samples were characterized [17,18] and gapless topological Dirac states could be confirmed at all thicknesses using ARPES directly after growth [17]. In low-temperature transport measurements, linear magnetoresistance was found in thin samples (BST 6 and BST 7), a further indication for topological transport. All samples exhibited WAL at low magnetic fields from which one 2D channel was derived. The mobility μ_s of the topological surface state was too low with 280 cm^2 V^{-1} s^{-1} to observe Shubnikov-de Haas oscillations at magnetic fields lower than 9 T [18].

III. RESULTS

In Fig. 2 the sheet resistance R_s during cooldown is shown for all sample thicknesses. Metallic behavior is dominant, except for the thinnest samples, BST 6 and BST 7, which are insulating between room temperature and 200 K, where they become metallic. At base temperature (300 mK) all samples are insulating, with the transition temperature between the metallic and insulating phase, T^*, found to be between 7 to 11 K, depending on the sample thickness [see inset in Fig. 2(a)].

The temperature range below T^* is explored in more detail in Fig. 3 for each sample thickness. The temperature was increased in small steps starting at a base temperature of 300 mK, taking care for the temperature to stabilize. An external magnetic field was swept between 0 and 0.5 T at each temperature step. Both longitudinal and transverse resistance were recorded from which the conductivity could be calculated. Only one field loop needed to be taken since the noise level was low.
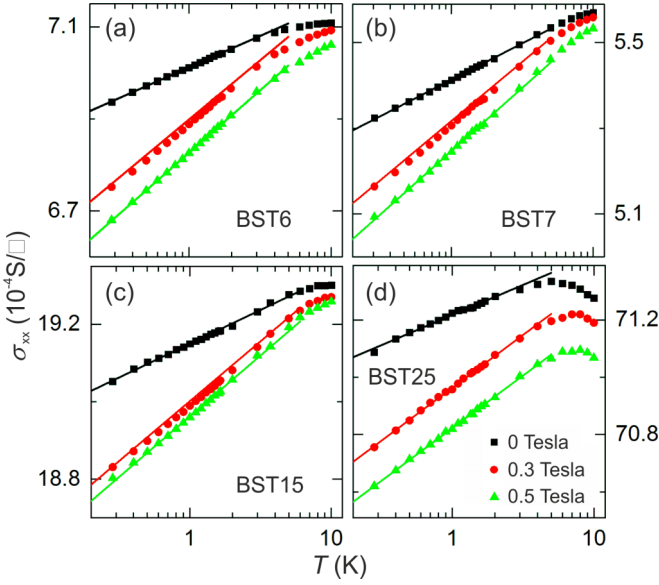
FIG. 3. (a)–(d) Longitudinal conductivity σ_{xx} of four different samples at low temperature for three different perpendicular magnetic fields. Using a logarithmic scale for the temperature, the linear regions are fitted using Eq. (1) (straight lines). The magnetic field leads to a change of slope, from which the screening and number of 2D channels can be derived.

IV. DISCUSSION

EEI originate from pairing of electrons at the Fermi energy and lead to a decrease in the carrier density, which in turn leads to a reduction of the conductivity. As can be seen in Fig. 3, the correction to conductivity due to EEI sets in below a transition temperature and exhibits a well-defined temperature dependence, given by [19]

$$\delta\sigma(T) = -\frac{e}{\pi h} n_{\text{EEI}}\left(1 - \frac{3}{4}F\right)\ln\left(\frac{T}{T^\star}\right), \qquad (1)$$

where n_{EEI} is the number of 2D channels, F the screening factor, and T^* the transition temperature. By applying Eq. (1) to the measured conductivity in Fig. 3 using T^* [see inset in Fig. 2(a)], we obtain $f = n_{\text{EEI}}(1 - 3/4 * F)$ from the slope of the temperature dependence. The overall change of the conductivity correction between base and transition temperature, $\delta\sigma_{5\text{K}} - \delta\sigma_{300\text{mK}}$, increases with sample thickness [see Fig. 4(a)].

Figure 4(b) shows the change of f when a magnetic field is applied perpendicular to the sample. The value of f is smaller than 1 without magnetic field but rises to values close or above 1 at fields ≈ 0.2 T. This abrupt change reflects the disruption of phase coherence due to the magnetic field, impacting WAL. At fields > 0.2 T, where WAL has disappeared [13,18], any change in conductivity can be attributed to EEI. The saturation magnetic field is given by $B_\phi = \hbar/4el_\phi^2 \approx 165/l_\phi^2$ where l_ϕ is the phase coherence, to be in the order of hundreds of nm [18], and B_ϕ in the order of tens of milliTesla. Thus, 0.2 Tesla is an upper boundary of what would be required to reach saturation. f saturates above this field [see Fig. 4(b)] and is employed to investigate the underlying EEI it originates from. The screening parameter F can be inferred from f if n_{EEI}, the
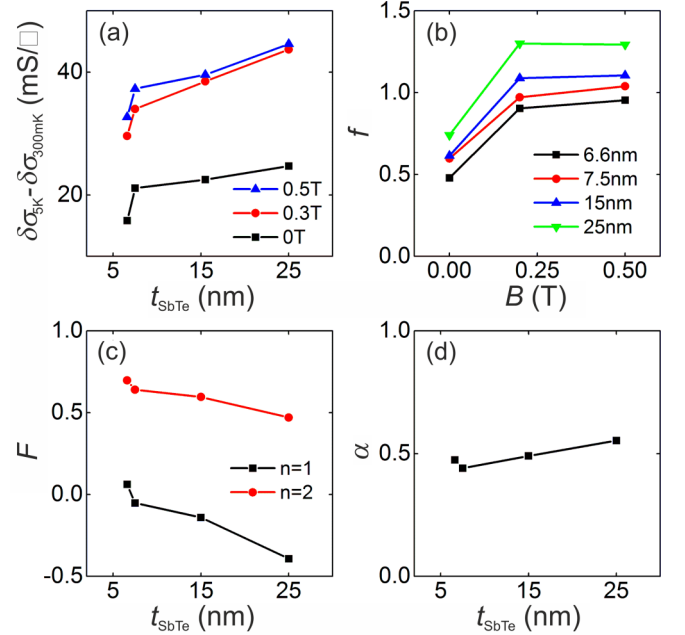

FIG. 4. (a) Difference of conductivity correction $\delta\sigma$ between 5 K and base temperature as a function of the Sb_2Te_3 thickness. (b) Change of the slope f with an external, perpendicular magnetic field, as shown in Fig. 3. (c) The screening factor F calculated from $f = n(1 - 3/4 * F)$, assuming the number of 2D states n is 1 (black squares) or 2 (red circles). The screening is negative for $n = 1$ and between 0 and 1 for $n = 2$, supporting the presence of more than one 2D channel. (d) Number of 2D channels α from WAL, obtained as described in the text. A value of 0.5 corresponds to one 2D channel.

number of 2D channels is known. F can attain values between 0 (no screening) and 1 (strong screening), a condition which cannot be fulfilled when f is larger than 1 and $n_{\text{EEI}} = 1$. Wu *et al.* [27] observe negative screening factors in TiAl alloys doped with heavy Au atoms and attribute it to the stronger spin-orbit coupling. Whether the same explanation is valid for TI awaits further theoretical investigation. As stated before, we allow for an integer prefactor n_{EEI} in Eq. (1), which—if chosen larger than 1—ensures that F stays in the physical range between 0 and 1. Here, n_{EEI} is the number of transport channels contributing to EEI independently. Hence, to obtain an F within the allowed range from our experimental results [29] we assume that $n_{\text{EEI}} > 1$ [see Fig. 4(c)].

For $n_{\text{EEI}} = 2$ the screening factor F decreases with thickness, from 0.73 for BST6 to 0.5 for BST25 [see Fig. 4(c)]. It cannot be excluded that $n_{\text{EEI}} > 2$, but although the values of F differ, the thickness dependence remains unchanged. This goes hand-in-hand with a similar thickness-dependent increase of the conductivity correction, since weaker screening means stronger EEI, hence larger $\delta\sigma$. In single layers, both a decrease [34,36] as well as an increase [39] of F with increasing thickness have been reported. The increase was attributed to a stronger screening due to the bulk states in thicker samples [39].

To explain our results in light of these contradicting earlier observations, we derived a semiclassical Boltzmann theory for the topological *p-n* junctions. The total conductivity [see Eqs. (C18) and (C19) in the Supplemental Material [40] for

its derivation] is given by

$$
\overleftrightarrow{\sigma}_{\text{tot}}(\boldsymbol{B}) = e\,\overleftrightarrow{\bar{\mu}}_{\text{v}}^{\parallel}(\boldsymbol{B})N_A A_h
$$

$$
\times \left[(L_A - W_p) + \int_0^{W_p} dz \, \exp\left(-\frac{\beta e \bar{\mu}_h N_A}{2\epsilon_0 \epsilon_r D_h} z^2 \right) \right]
$$

$$
- e\,\overleftrightarrow{\bar{\mu}}_{\text{c}}^{\parallel}(\boldsymbol{B})N_D A_e
$$

$$
\times \left[(L_D - W_n) + \int_0^{W_n} dz \, \exp\left(-\frac{\beta e \bar{\mu}_e N_D}{2\epsilon_0 \epsilon_r D_e} z^2 \right) \right]
$$

$$
+ e\,\overleftrightarrow{\bar{\mu}}_{\text{s}}^{\pm}(\boldsymbol{B})\left(\frac{\alpha_0 \Delta_0}{2\pi \hbar^2 v_F^2} \right)(L_A - L_0)A_s, \qquad (2)
$$

where $A_s = \tau_s/\tau_{sp}$ and $A_{e,h} = \tau_{e,h}/\tau_{p(e,h)}$. τ_s and $\tau_{e,h}$ are the energy relaxation and τ_{sp} and $\tau_{p(e,h)}$ the momentum relaxation time of the surface and bulk, respectively. $L_{A,D}$, $N_{A,D}$, $\bar{\mu}_{h,e}$,

$W_{p,n}$, and $D_{h,e}$ are thickness, electron density, mobility, range of depletion zone, and diffusion coefficient of the acceptor (donator) layer, respectively. v_F is the Fermi velocity of the surface states which are allowed to have a small band gap Δ_0 due to hybridization at small thicknesses. α_0 and L_0 are constants to be determined experimentally. The surface mobility is

$$
\overleftrightarrow{\bar{\mu}}_{\text{s}}(\boldsymbol{B}) = \frac{\mu_1}{1 + \mu_1^2 B^2} \begin{bmatrix} 1 & \mu_1 B \\ -\mu_1 B & 1 \end{bmatrix}, \qquad (3)
$$

with $\mu_1 = e\tau_{sp}v_F^2/\Delta_0 = e\tau_{sp}v_F^2/2k_B T_0$. For weak magnetic field, we have $\mu_1 B \ll 1$, $\mu_{xx} = \mu_{yy} = \mu_1$ and $\mu_{xy} = -\mu_{yx} = \mu_{21}B$.

When $B \to 0$ the conductance correction (see Eq. (C20) in the Supplement Material [40]) is given by

$$
\delta\sigma(T_e, u_s) \equiv \sigma_{\text{tot}}(T_e, u_s) - \sigma_{\text{tot}}^{(0)}(T_e, u_s) = -\mu_0^s\left(\frac{\alpha_0 \Delta_0}{2\pi\hbar^2 v_F^2} \right)(L_A - L_0)\left[\frac{\tau_0^s(T_e, u_s)}{\tau_0^s(T_e, u_s) + \tau_{\text{pair}}^s(T_e, u_s)} \right] \approx -\sigma_0^s\left[\frac{\tau_0^s(T_e, u_s)}{\tau_{\text{pair}}^s(T_e, u_s)} \right], \quad (4)
$$

where $\mu_0^s = e\tau_0^s v_F^2/\Delta_0 = e\tau_0^s v_F^2/2k_B T^*$, σ_0^s, and τ_0^s are the mobility, conductivity, and energy-relaxation time, respectively, of surface electrons in the absence of EEI.

Here, $\tau_{\text{pair}}^s(T_e, u_s)$ is the additional electron-electron pair scattering contribution to the inverse energy relaxation time (see Eqs. (C16) and (C17) in the Supplemental Material [40]), given by

$$
\frac{1}{\tau_{\text{pair}}^s(T_e, u_s)} = \frac{1}{n_0 \mathcal{A}}\sum_{\mathbf{k}_\parallel} \frac{f_{\mathbf{k}_\parallel}^s}{\tau_{\text{pair}}^s(\mathbf{k}_\parallel)} \approx \frac{1}{16\pi^4 \hbar n_0}\left(\frac{e^2}{2\epsilon_0 \epsilon_b} \right)^2 \int_{q_0}^{1/\delta_s} \frac{dq_\parallel}{q_\parallel}\left\{ 1 - \left(\frac{e^2 q_\parallel}{2\epsilon_0 \epsilon_b} \right)\frac{32 k_B T^*}{\pi \hbar^2 \Gamma_0^2}\left(\frac{T^*}{T_e} \right)D \right\}\int d^2\mathbf{k}_\parallel\, f_{\mathbf{k}_\parallel}^s
$$

$$
\times \int d^2\mathbf{k}_\parallel'\left[f_{\mathbf{k}_\parallel'}^s\left(1 - f_{\mathbf{k}_\parallel^-}^s \right)\left(1 - f_{\mathbf{k}_\parallel'^+}^s \right) + f_{\mathbf{k}_\parallel^-}^s f_{\mathbf{k}_\parallel'^+}^s\left(1 - f_{\mathbf{k}_\parallel'}^s \right) \right]\frac{\Gamma_0/\pi}{\left(\varepsilon_{\mathbf{k}_\parallel}^s + \varepsilon_{\mathbf{k}_\parallel'}^s - \varepsilon_{\mathbf{k}_\parallel^-}^s - \varepsilon_{\mathbf{k}_\parallel'^+}^s \right)^2 + \Gamma_0^2}, \qquad (5)
$$

where

$$
f_{\mathbf{k}_\parallel}^s \approx \frac{2\pi\hbar^2 v_F^2 n_0}{(k_B T_e)^2(1 + \Delta_0/k_B T_e)}\,\exp\left(-\frac{\varepsilon_{\mathbf{k}_\parallel}^s - \Delta_0}{k_B T_e} \right),
$$

and $n_0 = (m_s^*/2\pi\hbar^2)E_F^s = (\Delta_0/2\pi\hbar^2 v_F^2)E_F^s = (k_B T^*/\pi\hbar^2 v_F^2)$ $E_F^s \sim \alpha_0(L_A - L_0)$. We use $\gamma = +1$ and $q_0 = \Gamma_0/\hbar v_F$ as a cutoff for $q_\parallel \to 0$. $\mathbf{k}_\parallel^{\pm}$ stands for $\mathbf{k}_\parallel \pm \mathbf{q}_\parallel$ and $D = C_0 + \ln(T_e/T^*) - 1/2\ln 2(T_e/T^*)^2$. Here, pair scattering of bulk electrons will lead to reduction of total conductivity.

Important conclusions can be drawn from these theoretical results. Firstly, for a weak magnetic field B, the longitudinal conductivity becomes independent of B, although the Hall conductivity depends on B [see Eqs. (2) and (3)]. Furthermore, Eq. (5) for the energy relaxation time indicates that both pair scattering and screening effects from EEI do not depend on B. This is one more strong argument in favor of analyzing EEI by applying a weak magnetic field, in order to separate quantum corrections due to WAL from $\delta\sigma$ [see Eq. (1) and Fig. 4(b)].

Secondly, the experimentally found strong increase of EEI with the sample thickness [see Fig. 4(a)] can be directly derived from the theory. Equation (4) gives the dominant EEI-induced change in surface longitudinal conductivity at low B fields and reveals its thickness dependence. On one hand, we know that $\delta\sigma \propto \sigma_0^s \sim (L_A - L_0)$. On the other hand, we find that the ratio $\tau_0^s/\tau_{\text{pair}}^s \propto n_0 \sim (L_A - L_0)$. Overall, $\delta\sigma \propto$

$(L_A - L_0)^2$ which for $(L_A - L_0)/L_0 \ll 1$ leads to $\delta\sigma \propto L_A$. This linear relationship describes our experimental findings remarkably well [see Fig. 4(a)]. Finally, bulk electrons can also screen impurity scattering of surface electrons, but it becomes insignificant due to the large separation between the surface layer and the center of film.

The fact that $n_{\text{EEI}} = 2$ indicates that two independent 2D channels are involved and stands in contrast to the results of WAL measurements (see Ref. [18] and Fig. 4(d)). This discrepancy between WAL and EEI has been reported in Cu-doped BiSe single layers [29] and attributed to a 2D bulk state. For Sb_2Te_3 single layers [37], it was speculated that one coupled state of top and bottom TSS dominates WAL, but that they contribute independently to EEI. It is not clear how coupling could be mediated in our bilayer samples, since the depletion layer at the interface separates the Sb_2Te_3 and Bi_2Te_3 layer. Therefore, it is more likely that the 2D bulk plays a role in EEI processes in our samples.

Lastly, we determine the WAL contribution from the difference between the saturated and zero field amplitude Δf. We have shown already that EEI is independent of the magnetic field, and thus the change of the slope of $\delta\sigma$ with and without applied field can be attributed to WAL alone. The number of 2D states can be calculated using $\Delta f = p \times \alpha$. We obtain $p = 1$ from the temperature dependence of the coherence length l_ϕ (see Ref. [18]), commensurate with the EEI effect.

Lower values than 1 have been reported in the decoupled surface-transport regime [41]. It has to be mentioned that in the case of a substantial deviation of α from 0.5, the values of dephasing length and prefactor α extracted from the fits to the Hikami-Larkin-Nagaoka [24] equation may not be reliable due to the interchannel coupling effect [42]. We obtain $\alpha \approx 0.5$, i.e., that only one TSS is present at all thicknesses [18,38,39] [see Fig. 4(d)]. Since a TSS on the top surface has been confirmed in ARPES experiments [17], we conclude that the TSS at the bottom must be disrupted.

In summary, topological p-n junctions exhibit a rich set of transport characteristics related to their topological surfaces states. At low temperature, WAL and EEI compete in reducing the conductivity. The fact that EEI are unaffected by an external magnetic field was taken advantage of to determine the number of 2D channels. While exactly one was found from WAL, at least two are contributing to EEI. The growing presence of bulk states does not lead to stronger screening. On the contrary, conductivity corrections due to EEI strengthen with increasing thickness. This effect could be understood within a semiclassical Boltzmann theory.

[1] M. Z. Hasan and C. L. Kane, Rev. Mod. Phys. **82**, 3045 (2010).

[2] F. D. M. Haldane, Phys. Rev. Lett. **61**, 2015 (1988).

[3] R. Yu, W. Zhang, H. J. Zhang, S. C. Zhang, X. Dai, and Z. Fang, Science **329**, 61 (2010).

[4] C. Z. Chang, J. Zhang, X. Feng, J. Shen, and Z. Zhang, Science **340**, 167 (2013).

[5] J. G. Analytis, R. D. McDonald, S. C. Riggs, J. H. Chu, G. S. Boebinger, and I. R. Fisher, Nat. Phys. **6**, 960 (2010).

[6] J. G. Checkelsky, Y. S. Hor, R. J. Cava, and N. P. Ong, Phys. Rev. Lett. **106**, 196801 (2011).

[7] A. A. Taskin, S. Sasaki, K. Segawa, and Y. Ando, Phys. Rev. Lett. **109**, 066803 (2012).

[8] Y. L. Chen, J. G. Analytis, J. H. Chu, Z. K. Liu, S. K. Mo, X. L. Qi, H. J. Zhang, D. H. Lu, X. Dai, Z. Fang, S. C. Zhang, I. R. Fisher, Z. Hussain, and Z. X. Shen, Science **325**, 178 (2009).

[9] D. Kong, Y. Chen, J. J. Cha, Q. Zhang, J. G. Analytis, K. Lai, Z. Liu, S. S. Hong, K. J. Koski, S. K. Mo, Z. Hussain, I. R. Fisher, Z. X. Shen, and Y. Cui, Nat. Nanotechnol. **6**, 705 (2011).

[10] J. Zhang, C. Z. Chang, Z. Zhang, J. Wen, X. Feng, K. Li, M. Liu, K. He, L. Wang, X. Chen, Q. K. Xue, X. Ma, and Y. Wang, Nat. Commun. **2**, 574 (2011).

[11] C. Weyrich, M. Droegeler, J. Kampmeier, M. Eschbach, G. Mussler, T. Merzenich, T. Stoica, I. E. Batov, J. Schubert, L. Plucinski, B. Beschoten, C. M. Schneider, C. Stampfer, D. Grützmacher, and T. Schaepers, J. Phys.: Condens. Matter **28**, 495501 (2016).

[12] J. Chen, H. J. Qin, F. Yang, J. Liu, T. Guan, F. M. Qu, G. H. Zhang, J. R. Shi, X. C. Xie, C. L. Yang, K. H. Wu, Y. Q. Li, and L. Lu, Phys. Rev. Lett. **105**, 176602 (2010).

[13] J. Chen, X. Y. He, K. H. Wu, Z. Q. Ji, L. Lu, J. R. Shi, J. H. Smet, and Y. Q. Li, Phys. Rev. B **83**, 241304 (2011).

[14] H. Steinberg, J. B. Laloë, V. Fatemi, J. S. Moodera, and P. Jarillo-Herrero, Phys. Rev. B **84**, 233101 (2011).

[15] Y. Jiang, Y. Wang, M. Chen, Z. Li, C. Song, K. He, L. Wang, X. Chen, X. Ma, and Q. K. Xue, Phys. Rev. Lett. **108**, 016401 (2012).

[16] Z. Zhang, X. Feng, M. Guo, Y. Ou, J. Zhang, K. Li, L. Wang, X. Chen, Q. Xue, X. Ma, K. He, and Y. Wang, Phys. Status Solidi RRL **7**, 142 (2013).

[17] M. Eschbach, E. Młyńczak, J. Kellner, J. Kampmeier, M. Lanius, E. Neumann, C. Weyrich, M. Gehlmann, P. Gospodarič, S. Döring, G. Mussler, N. Demarina, M. Luysberg, G. Bihlmayer, T. Schäpers, L. Plucinski, S. Blügel, M. Morgenstern, C. M. Schneider, and D. Grützmacher, Nat. Comm. **6**, 8816 (2015).

[18] D. Backes, D. Huang, R. Mansell, M. Lanius, J. Kampmeier, D. Ritchie, G. Mussler, G. Gumbs, D. Grützmacher, and V. Narayan, Phys. Rev. B **96**, 125125 (2017).

[19] P. A. Lee and T. V. Ramakrishnan, Rev. Mod. Phys. **57**, 287 (1985).

[20] B. L. Altshuler, A. G. Aronov, and D. E. Khmelnitsky, J. Phys. C: Sol. St. Phys. **15**, 7367 (1998).

[21] E. J. König, P. M. Ostrovsky, I. V. Protopopov, I. V. Gornyi, I. S. Burmistrov, and A. D. Mirlin, Phys. Rev. B **88**, 035106 (2013).

[22] H. Z. Lu and S. Q. Shen, Phys. Rev. Lett. **112**, 146601 (2014).

[23] J. G. Checkelsky, Y. S. Hor, M. H. Liu, D. X. Qu, R. J. Cava, and N. P. Ong, Phys. Rev. Lett. **103**, 246601 (2009).

[24] S. Hikami, A. I. Larkin, and Y. Nagaoka, Prog. Theor. Phys. **63**, 707 (1980).

[25] T.-A. Nguyen, D. Backes, A. Singh, R. Mansell, C. Barnes, D. A. Ritchie, G. Mussler, M. Lanius, D. Grützmacher, and V. Narayan, Sci. Rep. **6**, 27716 (2016).

[26] V. Narayan, T.-A. Nguyen, R. Mansell, D. Ritchie, and G. Mussler, Phys. Status Solidi RRL **10**, 253 (2016).

[27] C. Y. Wu, W. B. Jian, and J. J. Lin, Phys. Rev. B **52**, 15479 (1995).

[28] J. Wang, A. M. DaSilva, C. Z. Chang, K. He, J. K. Jain, N. Samarth, X. C. Ma, Q. K. Xue, and M. H. W. Chan, Phys. Rev. B **83**, 245438 (2011).

[29] Y. Takagaki, A. Giussani, K. Perumal, R. Calarco, and K. J. Friedland, Phys. Rev. B **86**, 125137 (2012).

[30] S. P. Chiu and J. J. Lin, Phys. Rev. B **87**, 035122 (2013).

[31] A. Roy, S. Guchhait, S. Sonde, R. Dey, T. Pramanik, A. Rai, H. C. P. Movva, L. Colombo, and S. K. Banerjee, Appl. Phys. Lett. **102**, 163118 (2013).

[32] Y. Takagaki, U. Jahn, A. Giussani, and R. Calarco, J. Phys. Condens. Matter **26**, 95802 (2014).

[33] R. Dey, T. Pramanik, A. Roy, A. Rai, S. Guchhait, S. Sonde, H. C. P. Movva, L. Colombo, L. F. Register, and S. K. Banerjee, Appl. Phys. Lett. **104**, 223111 (2014).

[34] A. Y. Kuntsevich, A. A. Gabdullin, V. A. Prudkogliad, Y. G. Selivanov, E. G. Chizhevskii, and V. M. Pudalov, Phys. Rev. B **94**, 235401 (2016).

[35] P. Sahu, J. Y. Chen, J. C. Myers, and J. P. Wang, Appl. Phys. Lett. **112**, 122402 (2018).

[36] W. J. Wang, K. H. Gao, and Z. Q. Li, Sci. Rep. **6**, 25291 (2016).

[37] Y. Takagaki, B. Jenichen, U. Jahn, M. Ramsteiner, and K. J. Friedland, Phys. Rev. B **85**, 115314 (2012).

[38] Y. Jing, S. Huang, K. Zhang, J. Wu, Y. Guo, H. Peng, Z. Liu, and H. Q. Xu, Nanoscale **8**, 1879 (2016).

[39] T. Trivedi, S. Sonde, H. C. P. Movva, and S. K. Banerjee, J. Appl. Phys. **119**, 055706 (2016).

[40] See Supplemental Material at http://link.aps.org/supplemental/10.1103/PhysRevB.99.125139, which includes Refs. [18,43–47], for the derivation of the semiclassical Boltzmann theory.

[41] J. Liao, J. Ou, H. Liu, K. He, X. Ma, Q.-K. Xue, and Y. Li, Nat. Comm. **8**, 16071 (2017).

[42] I. Garate and L. Glazman, Phys. Rev. B **86**, 035422 (2012).

[43] Q. Niu, M.-C. Chang, B. Wu, D. Xiao, and R. Cheng, *Physical Effects of Geometric Phases* (World Scientific Publishing Co. Pte. Ltd., Singapore, 2017).

[44] A. Iurov, G. Gumbs, and D. H. Huang, Phys. Rev. B **98**, 075414 (2018).

[45] D. H. Huang and M. O. Manasreh, Phys. Rev. B **54**, 2044 (1996).

[46] D. H. Huang, P. M. Alsing, T. Apostolova, and D. A. Cardimona, Phys. Rev. B **71**, 195205 (2005).

[47] X. L. Lei and C. S. Ting, Phys. Rev. B **32**, 1112 (1985).